BEHAVIOR EVALUATION FOR REINFORCED CONCRETE COLUMNS WITH RECTANGULAR HOLLOW SECTION SUBJECTED TO AXIAL COMPRESSION AND BIAXIAL BENDING

Zigang Xu[1], Qiang Han[2✉], Chao Huang[3]

[1, 2]*Key Laboratory of Urban Security and Disaster Engineering of Ministry of Education,*
Beijing University of Technology, No. 100 Pingleyuan, Chaoyangg District, 100124 Beijing, China
[3]*Dept of Civil, Structural and Environmental Engineering,*
The State University of New York at Buffalo, 12 Capen Hall, Buffalo, NY 14260, USA
E-mails: [1]xzg@emails.bjut.edu.cn; [2]qhan@bjut.edu.cn; [3]chaohuan@buffalo.edu

Abstract. In order to evaluate the behavior of reinforced concrete columns with rectangular hollow section subjected to axial compression and biaxial bending, the calculation formula of load capacity and moment-curvature relationship are derived according to the distribution type of neutral axis in this paper. The load capacity and rotation ductility of the bottom control section of three reinforced concrete specimen bridge columns with rectangular hollow section under different axial compression ratio, reinforcement ratio and stirrup ratio are analyzed based on these calculation formulae. The M_x–M_y interaction curves and moment-curvature curves of bridge column specimens derived from the theoretical calculation show good agreement with the experimental data obtained by cyclic testing of three specimens under axial compression and biaxial bending. The results show that the P–M_x–M_y interaction has considerable effects on the behavior of the reinforced concrete bridge columns with rectangular hollow section. If these interaction effects are ignored, then the load capacity and deformation are overestimated and this fact can be crucial from the viewpoint of design.

Keywords: biaxial bending, bridge column, deformation, load capacity, rectangular hollow section.

1. Introduction

Reinforced concrete (RC) bridge columns with rectangular hollow section (RHS) have been widely used in engineering practice, especially for bridge columns with high elevations. Hollow section columns offer an optimal strength/mass ratio and stiffness/mass ratio for bridges in seismic regions and reduce the mass contribution of the column to seismic response (Dong *et al.* 2014). And the other side, columns with RHS also reduce the tendency for thermally-induced cracking at an early age resulting from heat-of-hydration temperature variations (Han *et al.* 2013). Among Chinese bridge engineering, these RC columns with RHS are usually designed as in Fig. 1a what is recommended by *Chinese code JTJ004-89: Seismic Design Code of Highway Engineering.* However, some hollow columns were damaged seriously during 2008 Wenchuan earthquake in China (Han *et al.* 2009). Priestley *et al.* (1996) suggested that large amounts of transverse links and hoops for effective reinforcement of hollow cross section are required to enhance lateral resistance capacity what was adopted in the current *Chinese Code JTG/T B02-01*(2008)*: Guideline for Seismic Design of Highway Bridges,* as shown in Fig. 1b.

Although this configuration provides excellent confinement to the concrete, its construction practice is relatively complex and expensive compared to the conventional RC columns. Bridge columns are always designed in longitudinal and transverse following the current Chinese seismic design code for highway bridges (Wang *et al.* 2014). However, the section forms and reinforcement configurations of hollow columns are significantly different from RC solid columns (Hong 2001; Pinto *et al.* 2003). RC columns will be subjected to vertical loads and bidirectional horizontal loads under earthquake excitation. The solid RC column behavior subjected to axial compression and biaxial bending are different from those subjected to axial compression and uniaxial bending due to the bidirectional coupling effect (Chang 2010; Fafitis 2001; Qiu *et al.* 2002). The main objectives in this paper are: (1) to evaluate the behavior of RHS of RC columns subjected to axial compression and biaxial bending, (2) to offer a simple and effective method for safety verification on the hollow cross section considering the P–M_x–M_y interaction.

The load capacity equilibrium equations of RC columns under axial compression and biaxial bending were calculated based on the theory of "simplified rectangular

block", and load capacity of axial force and moment inte-raction relationship for different section forms have been carried out by Cengiz (1990). Di Ludovico *et al.* (2012) researched the experimental behavior of nonconforming RC columns with plain bars under constant axial load and biaxial bending. Stefan, Léger (2010) investigated multi-criteria capacity envelopes for biaxial bending of concrete hydraulic structures. However, there is few research referred to the achievements in load capacity and ductility evaluation of RC columns with RHS. According to the distribution of the neutral axis, the calculation formula of load capacity and curvature is derived in this paper based on the section feature, details of seismic design and stress conditions of existing RC bridge columns with RHS in China. The numerical calculation of bottom section of three RC rectangular hollow columns with different axial compression ratio, reinforcement ratio and stirrup ratio are analyzed based on these calculation formulas and then compared with the experiment results. The load capacity, ductility and its influence parameters of a rectangular hollow section of an existing bridge column have been analyzed, and the P–M_x–M_y interaction yield surface has also been developed in this paper.

2. Analysis of load capacity and deformation

2.1. Functional equation of P, M_x and M_y

The stress distribution of the rectangular hollow section under an axial force (P) and biaxial bending moments (M_x and M_y) are shown in Fig. 2. The theoretical model will be developed based on several assumptions, including: a) plane cross section assumption, b) concrete tension is ignore, c) the bond-slip between steel and concrete is not taken into account, d) shear deformation and torsional deformation are not considered. The section size of the hollow rectangular is $b \times h$ with wall-thickness of d and concrete cover thickness of c.

The depth of compression is R and the angle between neutral axis and x axis is φ. Concrete compressive zone

consists of external concrete cover, confined concrete core and internal concrete cover with the area of A_1, A_2 and A_3 respectively. The area of four triangles with the hypotenuse of l_1, l_2, l_3 and l_4 is S_1, S_2, S_3 and S_4 respectively.

$$l_1 = \frac{R}{\tan\varphi} + R\tan\varphi, \tag{1}$$

$$l_2 = \frac{R}{\tan\varphi} + R\tan\varphi - \frac{c}{\sin\varphi} - \frac{c}{\cos\varphi}, \tag{2}$$

$$l_3 = \frac{R}{\tan\varphi} + R\tan\varphi - \frac{c+d}{\sin\varphi} - \frac{c+d}{\cos\varphi}, \tag{3}$$

$$l_4 = \frac{R}{\tan\varphi} + R\tan\varphi - \frac{2c+d}{\sin\varphi} - \frac{2c+d}{\cos\varphi}, \tag{4}$$

$$S_1 = \frac{R^2}{\sin 2\varphi}; \; S_2 = \left(\frac{l_2}{l_1}\right)^2 S_1; \; S_3 = \left(\frac{l_3}{l_1}\right)^2 S_1; \; S_4 = \left(\frac{l_4}{l_1}\right)^2 S_1, \tag{5}$$

$$A_1 = S_1 - S_2; \; A_2 = S_2 - S_3; \; A_3 = S_3 - S_4. \tag{6}$$

Equilibrium equations can now be written as follows:

$$P = f_c' A_1 + f_{cc}' A_2 + \sum_c A_{sci} f_{si} + \sum_t A_{sti} f_{si}, \tag{7}$$

$$M_x = f_c' A_1 \left(\frac{h}{2} - \frac{1}{3}\frac{R}{\cos\varphi}\right) - f_c' A_2 \left(\frac{h}{2} - c - \frac{1}{3}l_2\sin\varphi\right) +$$
$$f_{cc}' A_2 \left(\frac{h}{2} - c - \frac{1}{3}l_2\sin\varphi\right) - f_{cc}' A_3 \left(\frac{h}{2} - c - d - \frac{1}{3}l_3\sin\varphi\right) +$$
$$f_c' A_3 \left(\frac{h}{2} - c - d - \frac{1}{3}l_3\sin\varphi\right) - f_c' A_4 \left(\frac{h}{2} - 2c - d - \frac{1}{3}l_4\sin\varphi\right) +$$
$$\sum_c A_{sci} f_{si} y_i - \sum_t A_{sti} f_{si} y_i, \tag{8}$$
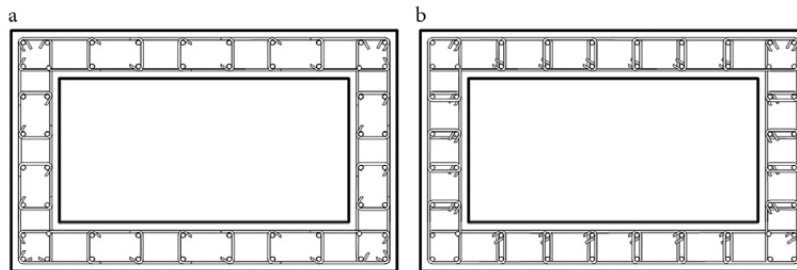
Fig. 1. Configurations of lateral reinforcement of RHS (Han *et al.* 2013): a – practice in China; b – suggested by JTG/T
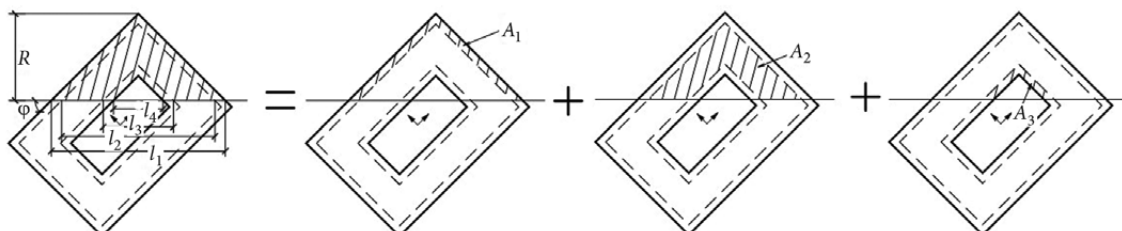
Fig. 2. Stress distribution of cross section

$$M_y = f_c' A_1 \left(\frac{b}{2} - \frac{1}{3} \frac{R}{\sin\varphi} \right) - f_c' A_2 \left(\frac{b}{2} - c - \frac{1}{3} l_2 \cos\varphi \right) +$$

$$f_{cc}' A_2 \left(\frac{b}{2} - c - \frac{1}{3} l_2 \cos\varphi \right) - f_{cc}' A_3 \left(\frac{b}{2} - c - d - \frac{1}{3} l_3 \cos\varphi \right) +$$

$$f_c' A_3 \left(\frac{b}{2} - c - d - \frac{1}{3} l_3 \cos\varphi \right) - f_c' A_4 \left(\frac{b}{2} - 2c - d - \frac{1}{3} l_4 \cos\varphi \right) +$$

$$\sum_c A_{sci} f_{si} x_i - \sum_t A_{sti} f_{si} x_i, \tag{9}$$

where f' – compressive strength of concrete cover, Pa; f_{cc}' – compressive strength of confined concrete core, Pa; f_{si} – tensile stress of No. i steel, Pa; A_{st} – the total area of the tensile reinforcement, m²; A_{sc} – the total area of the compression reinforcement, m².

Those mentioned equilibrium equations illustrate that the load capacity is related to only two geometric parameters, R and φ. Therefore they can also be written as follows:

$$P = f_1(R,\varphi); M_x = f_2(R,\varphi); M_y = f_3(R,\varphi). \tag{10}$$

Interaction between the axial force (P), and biaxial bending moments (M_x and M_y) is represented by a 3D surface based on the theories presented by Bresler (1960). If the load of a cross section is inside the 3D surface, the design will be acceptable. Otherwise the design of the cross section is not safe. There are three methods available to determine the biaxial strength of a column with RHS. These methods are listed as follows: (1) interaction curves for an assumed bending moment ratio; (2) load contours for an assumed axial load; (3) isogonic or three-dimensional curves as proposed by Marin (1979). The interaction curves (Lai *et al.* 1984; Rodriguez *et al.* 1999) obtained by these three methods are presented in Fig. 3.

2.2. Deformation of the rectangular hollow section

There is a corresponding sectional curvature for an assumed axial load (P) to the rectangular hollow bridge column. And the moment of this section which is corresponding with the curvature that is obtained based on the strain contribution of this cross section. By varying the strain values, a series of moments and curvatures will be calculated and the curve between moment and curvature can also be obtained. Similar to the calculation of load capacity, both unconfined concrete cover and confined concrete core should be considered in the analysis of moment-curvature, shown in Fig. 4.

Equilibrium equations can be written as follows:

$$P = \int_0^R \left[b_{c(x)} f_c(\varepsilon_x) + \left(b_{(x)} - b_{c(x)} \right) f_{cu}(\varepsilon_x) \right] dx +$$

$$\sum_{i=1}^n A_{si} f_s(\varepsilon_{xi}), \tag{11}$$

$$M = \int_0^R \left[b_{c(x)} f_c(\varepsilon_x) + \left(b_{(x)} - b_{c(x)} \right) f_{cu}(\varepsilon_x) \right] x dx +$$

$$\sum_{i=1}^n A_{si} f_s(\varepsilon_{xi}) x_i, \tag{12}$$

where $\varepsilon_x = \varepsilon_c \left(1 - \frac{x}{R} \right)$.

Then, the curvature can be written as that:

$$\varphi = \frac{\varepsilon_c}{R}. \tag{13}$$

The deformation of bridge column is shown in Fig. 5. Column height = L, m; length of plastic hinge = L_p, m; yield curvature of column section = φ_y, m⁻¹; ultimate curvature of column section = φ_u, m⁻¹; plastic curvature of column section $\varphi_p = \varphi_u - \varphi_y$, m⁻¹; plastic rotation $\theta_p = L_p \varphi_p$, non-dimensional. Then, yield displacement of column top section, plastic displacement of column top section and total displacement of column top section in horizontal can be calculated by the follow formulae.

$$\Delta_y = \frac{\varphi_y L^2}{3}, \tag{14}$$

$$\Delta_p = \theta_p \left(L - \frac{L_p}{2} \right) = L_p \left(\varphi_u - \varphi_y \right) \left(L - \frac{L_p}{2} \right), \tag{15}$$

$$\Delta_u = \Delta_y + \Delta_p = \frac{\varphi_y L^2}{3} + L_p \left(\varphi_u - \varphi_y \right) \left(L - \frac{L_p}{2} \right). \tag{16}$$
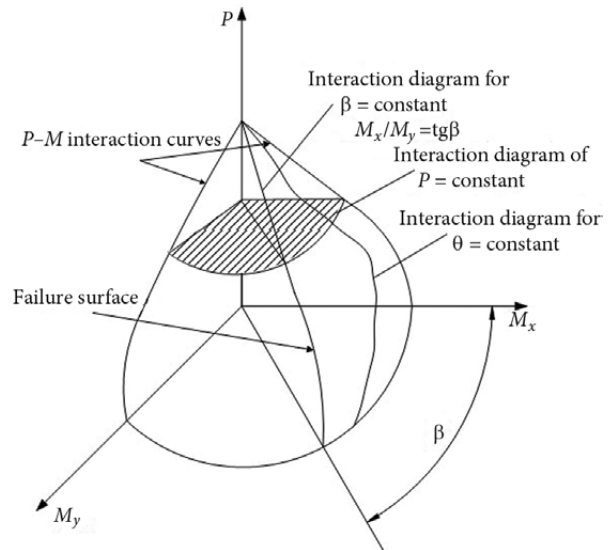
Fig. 3. Three-dimensional *P–M* the interaction yield surface
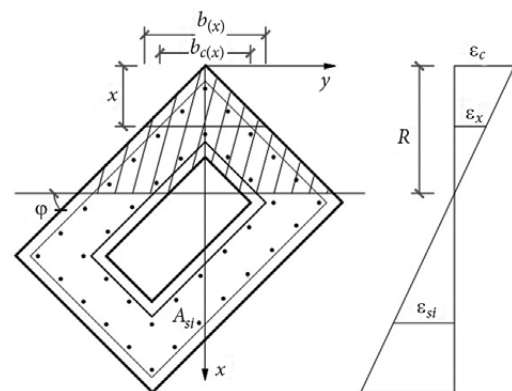
Fig. 4. *M–φ* Analytical diagram

The length of plastic hinge recommended by Priestley (1996) can be calculated as following:

$$L_p = 0.08L + 0.022 f_y d_s \geq 0.044 f_y d_s, \qquad (17)$$

where L – Column height, m; f_y – yield strength of longitudinal reinforcement, MPa; d_s – diameter of longitudinal reinforcement, m.
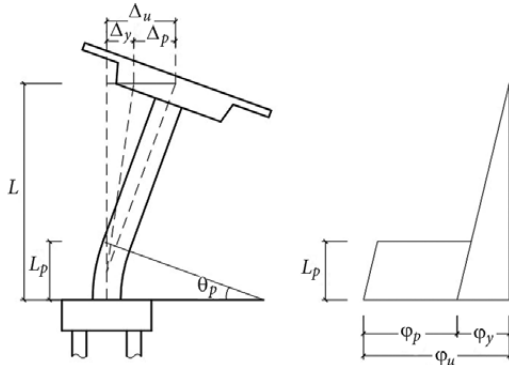
Fig. 5. Deformation of bridge columns
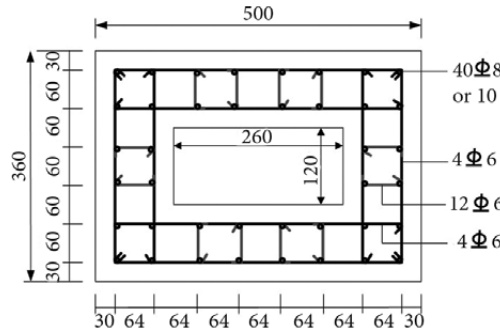
Fig. 6. Steel configuration of cross section, in mm

Table. 1. Properties of the column specimens

Column	Axial load, MN	η_k	Longitudinal reinforcement			Transverse reinforcement	
			Number	Diameter, mm	ρ_l	Spacing, mm	ρ_s
S1	0.28	0.1	40	8	0.014	40	0.035
S2	0.56	0.2	40	10	0.021	40	0.035
S3	0.28	0.1	40	10	0.021	55	0.025
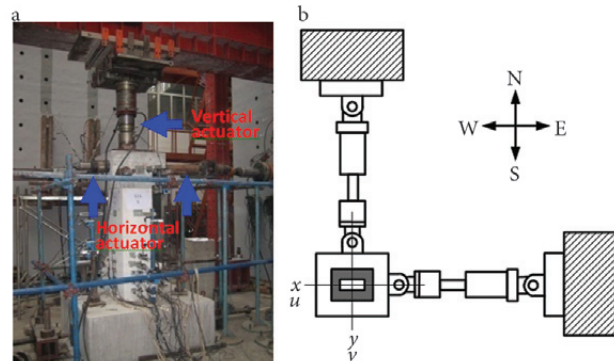
Fig. 7. Bilateral loading setup and protocol: a – test setup; b – Bi-directional loading diagram

3. Experiment and numerical simulation of RC RHS

3.1. Experiment program

The cross section of the specimen is 0.5×0.36 m, the wall thickness is 120 mm and the height of the column (distance from the top of the RC footing to the loading point) is 1.44 m. Fig. 6 shows the configuration and reinforcement of this rectangular hollow section. The properties of these specimens are listed in Table 1. S1 and S3 were tested under a constant axial load of $0.1 f_c' A_g$, and S2 was tested under a constant axial load of $0.2 f_c' A_g$, which is the estimated weight of the bridge deck. f_c' is the 28-day concrete compressive strength, and A_g is the gross section area of RHS. The experiment program was conducted in the *Key Laboratory of Urban Security and Disaster Engineering (KLUSDE) of Beijing University of Technology, China*. In this research, the prescribed bidirectional displacement cyclic loading protocols were defined based on a predetermined displacement history in terms of the column drift ratio. The lateral load correction scheme and the target lateral displacement history in two perpendicular horizontal directions are shown in Fig. 7. In this figure, two perpendicular axes (the weak axis and strong axis) at the top of column are defined as x axis and y axis, respectively and the corresponding displacements in x axis and y axis are denoted as u and v, respectively.

Compared with the prototype RC column, this research applied the same steel and concrete materials for the specimen, resulting in a stress scaling factor of 1.0. There were two different longitudinal reinforcing bars with diameter of 8 mm or 10 mm using in this experiment and the transverse reinforcing bars were 6 mm in diameter. A design yielding strength of all the reinforcing bars was 300 MPa. The design 28-day compressive strength for concrete f_c' was 19.1 MPa. the strength test of the steel and concrete coupons were conducted before which showed that the average measured values of the yielding strength, ultimate stress and ultimate strain of reinforcing steel coupons from standard tensile tests were 385 MPa, 498 MPa and 0.16, respectively. The actual average compressive strength of concrete was $f_{cu}' = 42.6$ MPa, which was determined by a typical 150×150×150 mm cubic compression test after 28-day curing process. Both the measured strengths of reinforcing steel and concrete were higher than the design strengths.

The displacements corresponding to the yield of a longitudinal steel bar are defined as the yield displacements of a column in x and y axes. Strain gauge measurements indicate that the longitudinal steel bars at the corners yielded first and the yield displacements are $u_y = 8.8$ mm and $v_y = 8.8$ mm for specimen S2, and the yield moments in two directions are found to be $M_{yx} = 222$ kN·m and $M_{yy} = 124$ kN·m. The flexural moment was calculated by the following equation:

$$M = F \cdot H + P \cdot \Delta, \qquad (23)$$

where F – a lateral load, that equals to the developed restoring force in the opposite direction, N; Δ – the corresponding

lateral displacement, m. Second-order effect (P–Δ effect) is included in this equation. Table 2 showed the experimental results of all these specimens.

3.2. Numerical simulation

The concrete is represented by a Mander *et al.* (1988) model and the steel reinforcement is represented by a bilinear strain hardening model as shown in Fig. 8.

When the unconfined concrete cover reaches its ultimate compression strain (0.004) or the reinforcement reaches the strain hardening stage (the corresponding tensile strain is 0.01), this section is defined as reaching the yield point.

The complete curve and ideal bilinear model between moment and curvature of these three specimens under a constant axial compression and biaxial bending are shown in Fig. 9. As shown in Fig. 9 and Table 2, skeleton curves

Table. 2. Feature points results of specimen columns

Column		Yield displacement, mm			Yield side force, kN			Ultimate displacement, mm			Ultimate side force, kN			Ultimate moment, kN·m		
		Test values	Calculate values	Error	Test values	Calculate values	Error	Test values	Calculate values	Error	Test values	Calculate values	Error	Test values	Calculate values	Error
S1	*x*-axis	8.6	4.64	46.0%	88	88.68	0.8%	30.3	27.61	8.9%	95	89.07	6.2%	145	136	6.2%
	y-axis	5.5	5.25	4.5%	135	144.8	7.3%	30.4	28.39	6.6%	147	149.34	1.6%	220	223	1.4%
S2	*x*-axis	8.8	8.36	5.0%	124	130.78	5.5%	38.4	34.85	9.2%	145	132.28	8.8%	231	210	9.1%
	y-axis	8.8	9.19	4.4%	222	220.73	0.6%	34.0	35.68	4.9%	225	220.85	1.8%	343	338	1.5%
S3	*x*-axis	8.6	9.82	14.2%	128	117.54	8.2%	36.5	34.90	4.4%	133	129.33	2.8%	203	196	3.4%
	y-axis	9.3	10.57	13.7%	137	177.11	29.3%	34.1	35.60	4.4%	195	181.97	6.7%	291	272	6.5%
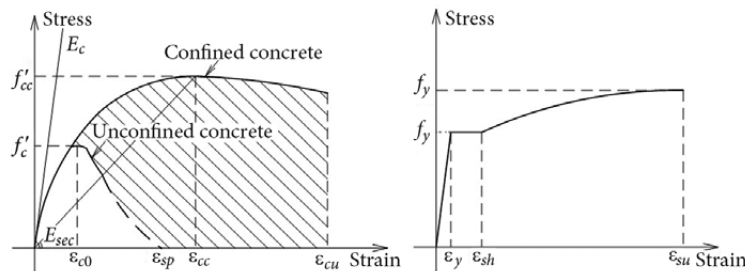
Fig. 8. Constitutive model of concrete and steel

a − *x*-direction of S1

c − *x*-direction of S2

e − *x*-direction of S3

b − *y*-direction of S1

d − *y*-direction of S2

f − *y*-direction of S3
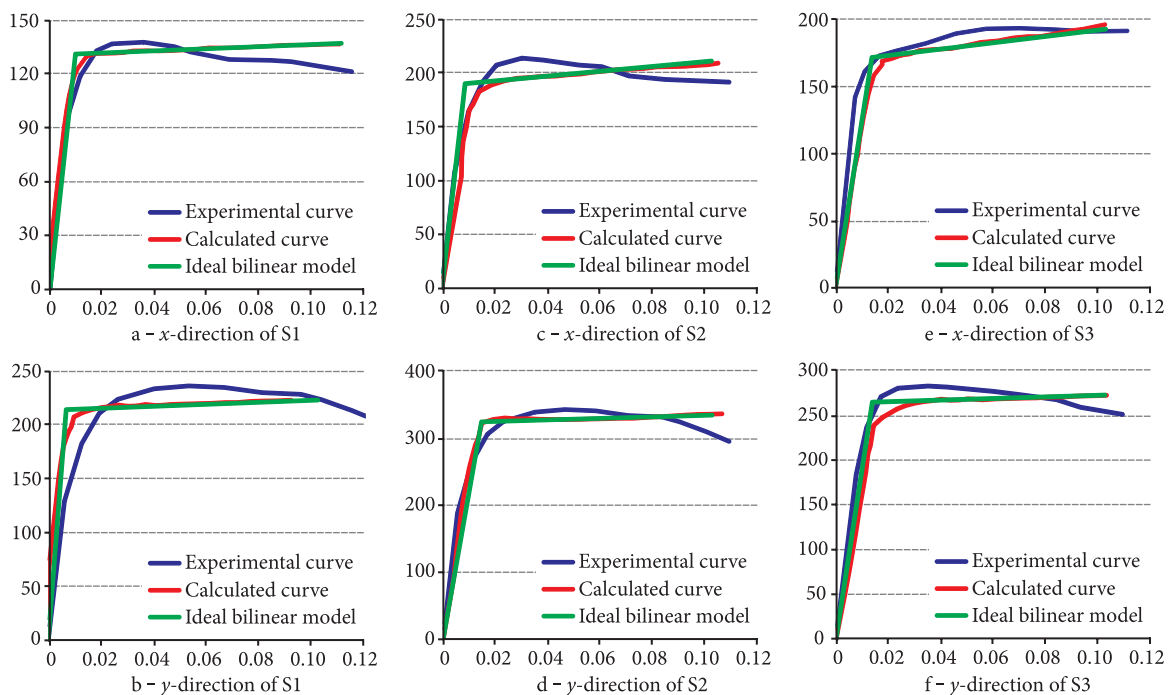
Fig. 9. Moment-curvature curves of specimen

of horizontal thrust and horizontal deformation of the top cross section and feature points on curves of moment and curvature of the bottom cross section in the experiment are similar to the theoretical results. The calculated and experimental values of yield displacement differed up to 13.8%, but the difference between calculated and experimental values of yield bearing capacity was less than 7% except for the specimen S3 the error of which was about 30%. The difference between calculated and experimental values of the ultimate horizontal bearing capacity was up to about 9%, while that of ultimate moment was less than 10%. Therefore, the theoretical model calculated by the method presented in this study agreed well with the experimental results, which will offer a simple and accurate method for practical engineering. At the same time, when the axial compression ratio of the three specimens were 0.1 or 0.2, the curves between M_x and M_y at ultimate state were obtained and shown in Fig. 10.

4. Comparative analysis of experimental and calculated results

The comparative of analysis of experimental and calculated results are also shown in Fig. 10. It is obvious that

experimental results of M_x and M_y at the ultimate state are outside of the calculated curves but not far from the curves. As shown in Fig. 11, the rupture of tensile longitudinal reinforcing bars at the bottom of the RC columns caused the ultimate failure mode for the specimens dominated by the flexural capacity of the RC columns. In addition, the value of M_y at the curves were larger than M_x in uniaxial compression bending which illustrated that y axis was strong axis of this rectangular hollow cross section and x axis was weak axis. The experimental and results of these three specimens, such as yield displacement, yield side force, ultimate displacement, ultimate side force and ultimate moment, are listed in Table 2.

5. Engineering application

5.1. Engineering situation

As shown in Fig. 12, the span arrangement of a continuous rigid frame bridge located in Beijing City in China, is 45+75+45+35 m. The concrete type of bridge column is C40 (i.e., the 28-day compression strength is 47.4 MPa). HRB335 steel was applied to the reinforcement with diameter over 12 mm while R235 steel is applied to the
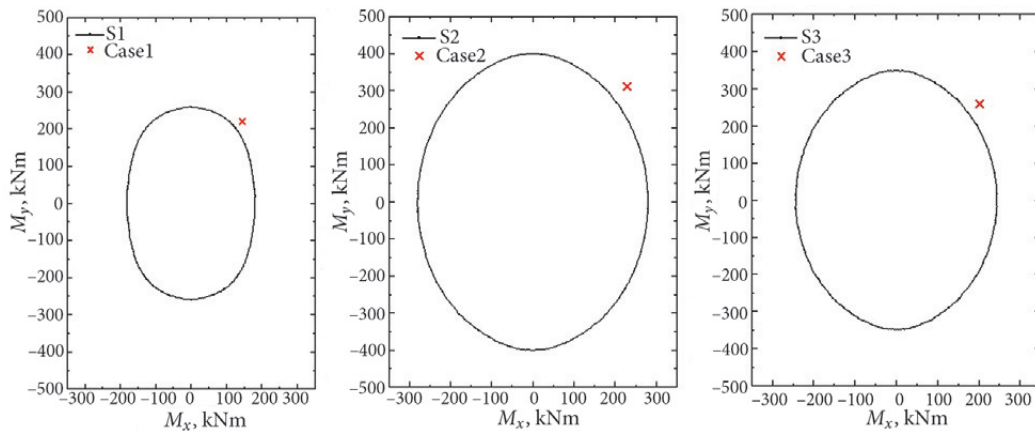
Fig. 10. Experimental and calculation results

Fig. 11. Failure modes of the specimen columns
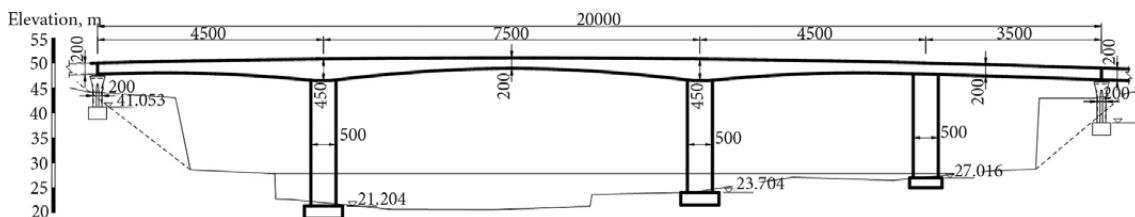
Fig. 12. Elevation diagram of bridge

reinforcement with diameter less than 12 mm. The highest column of this bridge is the second bent with 7 m × 5 m cross section dimension as shown in Fig. 13.

5.2. Analysis of load capacity

In order to compare the difference between uniaxial compression bending and biaxial compression bending, $P–M_x$ and $P–M_y$ curves at uniaxial compression bending and $M_x–M_y$ curve at constant axial compression were calculated in this section.

As shown in Fig. 14, these three cases may be obtained from three load combination cases in the practical project: I. $P = 4 \cdot 10^5$ kN, $M_x = 7.5 \cdot 10^5$ kN·m; II. $P = 4 \cdot 10^5$ kN, $M_y = 6.5 \cdot 10^5$ kN·m; III. $P = 4 \cdot 10^5$ kN, $M_x = 7.5 \cdot 10^5$ kN·m, $M_y = 6.5 \cdot 10^5$ kN·m. As shown in Figs 14a and 14b, the load points of cases I and II were both inside the curves, which illustrated that the cross section was safe to be used in these two cases. While in Fig. 13c, axial compression, moment in x direction and moment in y direction of case III were the same as cases I and II, but the load point was outside of the curve, which illustrated that the cross section would fail under the combination of the axial load and biaxial bending. The result shows that the coupling effect of M_x versus M_y will decrease the load capacity of bridge columns and the design method that only considers uniaxial bending is unsafe to estimate the load capacity.

5.3. 3D yield surface

3D interaction surface for the axial force P and the two bending moments M_x and M_y can be obtained by the method (2) load contours for a given axial load P, as shown in Fig. 15. This analytical method of 3D interaction surface was adapted by Lai et al. (1984) and Rodriguez et al. (1999). It is seen that there are two limit stages in $P–M_x–M_y$ interaction yield surface, one is axial load absence ($P = 0$), the yielding of the column under the interaction effects between M_x and M_y, but this stage is impossible in practical bridge engineering because of the weight of bridge superstructure P is never zero. The other is when the values of both M_x and M_y is equal to zero, meaning that the yielding of the column under maximum axial compression.

3D yield surface can be used to verify the safety of cross section in practical engineering. 2D curves of $M_x–M_y$ will be obtained at each axial compression based on the corresponding axial compression ratio. When the load point stays inside the 3D surface, the design will be considered as safe design. Otherwise the design is unsafe and it is necessary to re-design the cross section. Furthermore, it is obvious in Fig. 14 that when the axial compression ratio ranges from 0.2 to 0.4 (i.e., 160 000 kN to 320 000 kN), the area surrounded by the curve of $M_x–M_y$ is much larger than others. That is to say, at this case, the material properties are used in the optimal stage to resist the bending moment.
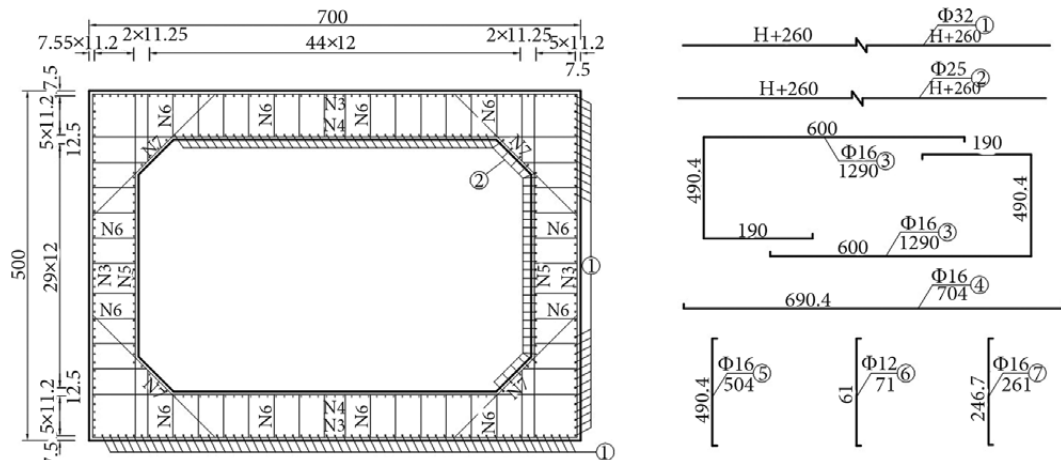
Fig. 13. Rectangular hollow cross section configurations and steel
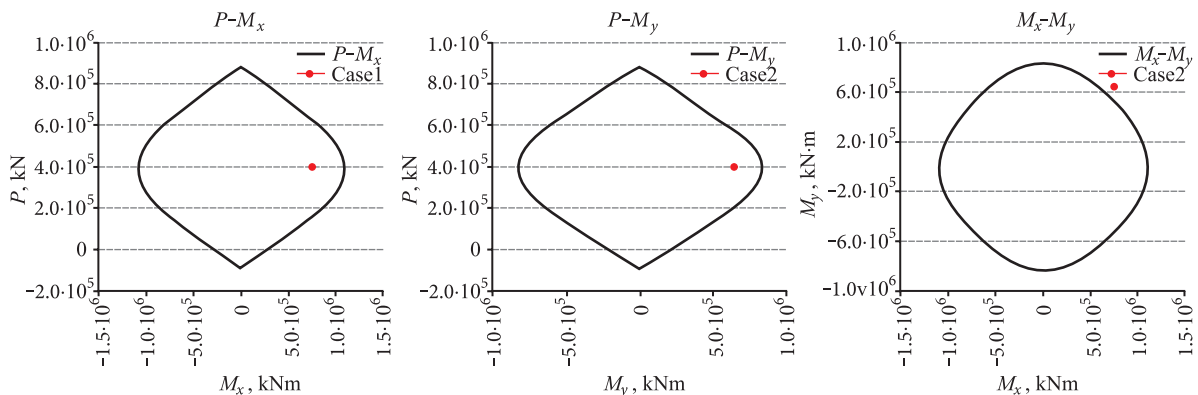
Fig. 14. Load capacity of control section under axial force and uniaxial and biaxial bending

5.4. Analysis of moment and curvature

When the angle between neutral axis and x axis range varies from 0° to 90°, the stress states of the section are different. As shown in Fig. 16, variation relationship between moment and curvature of the two principle axis are different.

As for the strong axis, x direction, the ultimate moment and curvature increase with the decreasing angle between neutral axis and x axis; as for the weak axis, y direction, the ultimate moment and curvature increase with the increasing angle. The amplitude of the increasing depends on the sectional properties.

6. Conclusion

The calculation formula of load capacity and curvature is derived according to the distribution of the neutral axis. The P–M_x–M_y interaction yield surfaces developed in this paper can be used in evaluating the load capacity and deformation of columns with rectangular hollow section. The following conclusions can be drawn:

1. The load capacity and the relationship between moment and curvature of rectangular hollow section

bridge column presented are accurate and reasonable. The moment-curvature curves of bridge column specimens derived from both the theoretical calculation and ideal bilinear model show good agreement with the experimental result. It is convenient and accurate to evaluate the behavior of rectangular hollow section bridge columns applying the bilinear model in practical bridge engineering.

2. There is significant overestimation of the load capacity and deformation if the P–M_x–M_y interaction effects are ignored and columns with hollow cross section are idealized independently in the transverse and longitudinal directions. The decrease in the load capacity and deformation due to bidirectional interaction is crucial, and must be included in the effective design of the columns with rectangular hollow section for the performance-based seismic design of bridges.

3. The M_x–M_y interaction curves in different axial compression ratio and three-dimensional yield surface calculation, developed in thi paper, offer a simple and effective method for safety verification of the cross section.

Acknowledgements

References

Bresler, B. 1960. Design Criteria for Reinforced Columns under Axial Load and Biaxial Bending, *ACI Journal Proceedings* 57(11): 481–490.
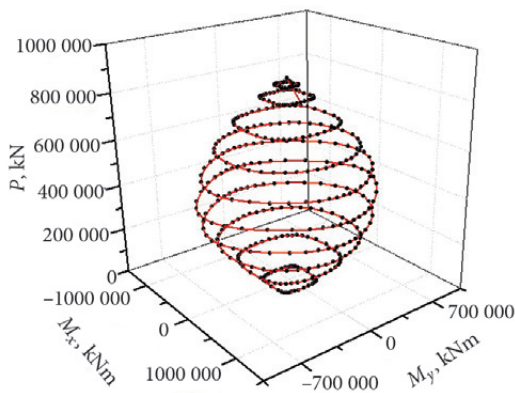
Fig. 15. P–M_x–M_y interaction yield surface
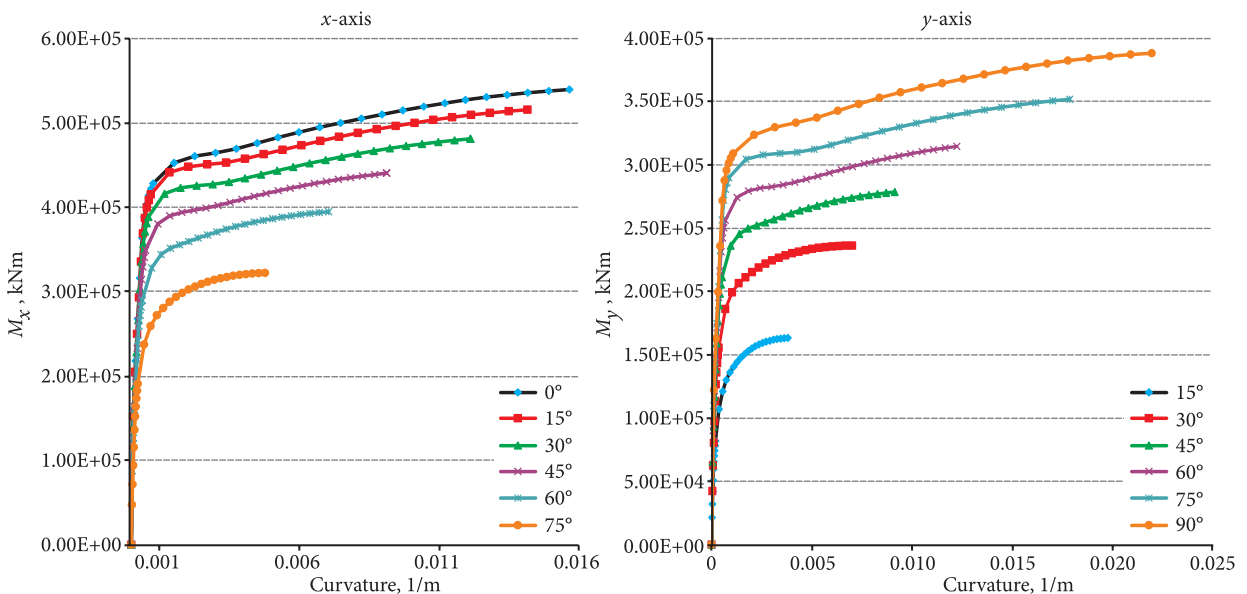
Fig. 16. M–φ curve with different angle

Cengiz, D. 1990. Concrete Box Sections under Biaxial Bending and Axial Load, *Journal of Structural Engineering* 116(3): 860–865. http://dx.doi.org/10.1061/(ASCE)0733-9445(1990)116:3(860)

Chang, S. Y. 2010. Experimental Studies of Reinforced Concrete Bridge Columns under Axial Load Plus Biaxial Bending, *Journal of Structural Engineering* 136(1): 12–25. http://dx.doi.org/10.1061/(ASCE)0733-9445(2010)136:1(12)

Di Ludovico, M.; Verderame, G. M.; Prota, A.; Manfredi, G.; Cosenza, E. 2012. Experimental Behavior of Nonconforming RC Columns with Plain Bars under Constant Axial Load and Biaxial Bending, *Journal of Structural Engineering* 139(6): 897–914. http://dx.doi.org/10.1061/(ASCE)ST.1943-541X.0000703

Dong, H. H.; Han, Q.; Du, X. L.; Wen, J. N. 2014. Multiple Shaking Tables Tests of Seismic Pounding Effect of Reinforced Concrete Bridge Model, *Journal of Vibroengineering* 16(7): 3565–3575.

Fafitis, A. 2001. Interaction Surfaces of Reinforced-Concrete Sections in Biaxial Bending, *Journal of Structural Engineering* 127(7): 840–846. http://dx.doi.org/10.1061/40513(279)12

Han, Q.; Du, X. L.; Liu, J. B.; Li, Z. X.; Li, L. Y.; Zhao, J. F. 2009. The Seismic Damage of Highway Bridges during 2008 Wenchuan Earthquake, *Earthquake Engineering and Engineering Vibration* 8(2): 263–273. http://dx.doi.org/10.1007/s11803-009-8162-0

Han, Q.; Du, X. L.; Zhou, Y. H.; Lee, G. C. 2013. Experimental Study of Hollow Rectangular Bridge Column Performance under Vertical and Cyclically Bilateral Loads, *Earthquake Engineering and Engineering Vibration* 12(3): 433–445. http://dx.doi.org/10.1007/s11803-013-0184-y

Hong, H. P. 2001. Strength of Slender Reinforced Concrete Columns under Biaxial Bending, *Journal of Structural Engineering* 127(7): 758–762. http://dx.doi.org/10.1061/(ASCE)0733-9445(2001)127:7(758)

Lai, S.; Will, G.; Otani S. 1984. Model for Inelastic Biaxial Bending of Concrete Members, *Journal of Structural Engineering* 110(11): 2563–2584. http://dx.doi.org/10.1061/(ASCE)0733-9445(1984)110:11(2563)

Mander, J.; Priestley, M.; Park, R. 1988. Theoretical Stress-Strain Model for Confined Concrete, *Journal of Structural Engineering* 114(8): 1804–1826. http://dx.doi.org/10.1061/(ASCE)0733-9445(1988)114:8(1804)

Marin, J. 1979. Design Aids for L-Shaped Reinforced Concrete Columns, *ACI Journal Proceedings* 76(11).

Pinto, A. V.; Molina, J; Tsionis, G. 2003. Cyclic Tests on Large-scale Models of Existing Bridge Piers with Rectangular Hollow Cross-Section, *Earthquake Engineering* & *Structural Dynamics* 32(13): 1995‒2012. http://dx.doi.org/10.1002/eqe.311

Priestley, M. J. N.; Seible, F.; Calvi, G. M. 1996. *Seismic Design and Retrofit of Bridges*. John Wiley & Sons, Inc., New York. 704 p. http://dx.doi.org/10.1002/9780470172858

Qiu, F.; Li, W.; Pan, P.; Qian, J. 2002. Experimental Tests on Reinforced Concrete Columns under Biaxial Quasi-Static Loading, *Engineering Structures* 24(4): 419–428. http://dx.doi.org/10.1016/S0141-0296(01)00108-0

Rodriguez, J. A.; Aristizabal-Ochoa, J. 1999. Biaxial Interaction Diagrams for Short RC Columns of Any Cross Section, *Journal of Structural Engineering* 125(6): 672–683. http://dx.doi.org/10.1061/(ASCE)0733-9445(1999)125:6(672)

Stefan, L.; Léger, P. 2010. Multicriteria Capacity Envelopes for Biaxial Bending of Concrete Hydraulic Structures, *Journal of Structural Engineering* 136(9): 1035–1043. http://dx.doi.org/10.1061/(ASCE)ST.1943-541X.0000205

Wang, P. G.; Han, Q.; Du, X. 2014. Seismic Performance of Circular RC Bridge Columns with Flexure-Torsion Interaction, *Soil Dynamics and Earthquake Engineering* (66): 13–30. http://dx.doi.org/10.1016/j.soildyn.2014.06.028